Supplement of Atmos. Chem. Phys., 25, 8831–8857, 2025
https://doi.org/10.5194/acp-25-8831-2025-supplement

Atmospheric Chemistry and Physics
Open Access

Supplement of

Modeling urban pollutant transport at multiple resolutions: impacts of turbulent mixing

Zining Yang et al.

Correspondence to: Chun Zhao (chunzhao@ustc.edu.cn)

Contents of this file

Figure S12: The spatial distributions of PBL mixing coefficient differences between high- and low-resolutions.

Figure S13: The spatial distributions of PBL mixing coefficient differences between the two higher-resolutions.

Figure S14: The latitude-pressure cross section of BC concentrations and wind flux across multi-resolutions along the USTC site.

Figure S15: The spatial distributions of friction velocity differences between high- and low-resolutions.

Figure S16: The spatial distributions of PBL mixing coefficient differences between high- and low-resolutions simulation results from the sensitivity experiments.

Figure S17: The spatial distributions of PBL mixing coefficient differences between the two higher-resolutions simulation results from the sensitivity experiments.

Figure S18: The latitude-pressure cross section of BC concentrations and wind flux across multi-resolutions from the sensitivity experiments along the USTC site.

Figure S19: The spatial distributions of BC column concentration differences between high- and low-resolutions.

Figure S20: The spatial distributions of BC column concentration differences between the two higher-resolutions.

Text S1. The process of grid refinement in this study.

Due to the disparate grid sizes of the three resolution simulations impeding direct calculation of spatial distribution differences, we employ a grid refinement method to upscale the low-resolution grids to match the high-resolution grid cells. The grid refinement process involves dividing the cells in the original coarse grid into finer cells. Specifically, the 25 km grids are divided into 25 x 25 small grids and the 5 km grids are divided into 5 x 5 small grids. This approach ensures that the grid resolution of all three simulations is identical while preserving spatial details, thus allowing us to quantify the differences between the 25 km resolution simulations and the two higher-resolution simulations.

Table S1. Description of land cover data classifications

Number	Description
1	Urban
2	Dryland cropland/pasture
3	Irrigated cropland/pasture
4	Mixed Dryland/Irrigated Cropland
5	Cropland/Grassland Mosaic
6	Cropland/Woodland Mosaic
7	Grassland
8	Shrubland
9	Mixed Shrubland/Grassland
10	Savanna
11	Deciduous Broadleaf Forest
12	Deciduous Needleleaf Forest
13	Evergreen Broadleaf Forest
14	Evergreen Needleleaf Forest
15	Mixed Forest
16	Water
17	Herbaceous Wetland
18	Wooded Wetland
19	Barren or Sparsely Vegetated
20	Herbaceous Tundra
21	Wooded Tundra
22	Mixed Tundra
23	Bare Ground Tundra
24	Snow or Ice

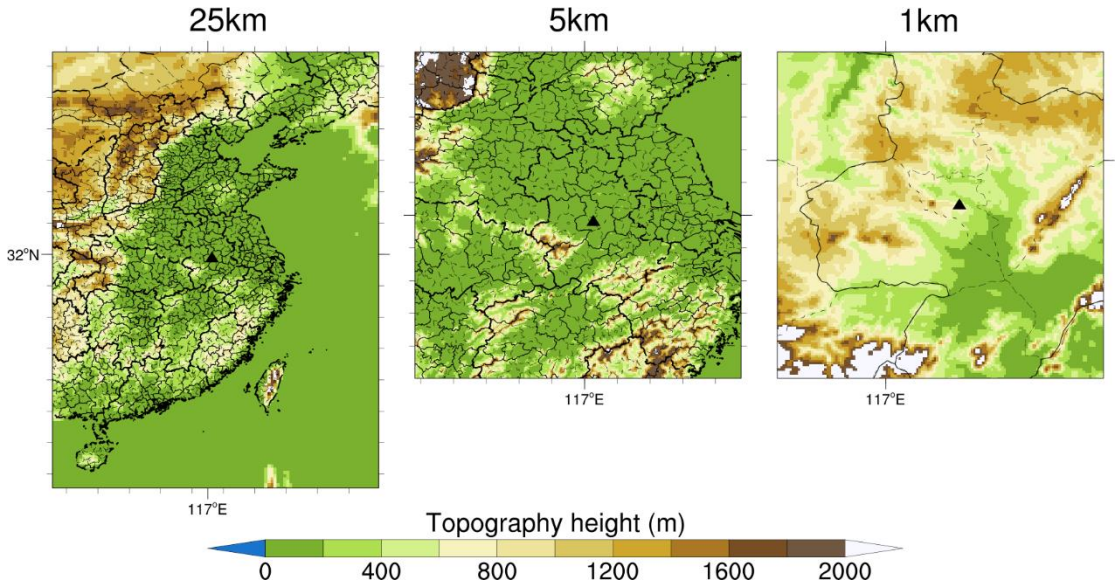

Figure S1. The three domains in the WRF-Chem simulations and the terrain height (m) of each domain. Domain one (D1) has a horizontal grid spacing of 25 km, domain 2 (D2) 5 km, and domain 3 (D3) 1 km. The solid black triangle indicates the location of the USTC site.

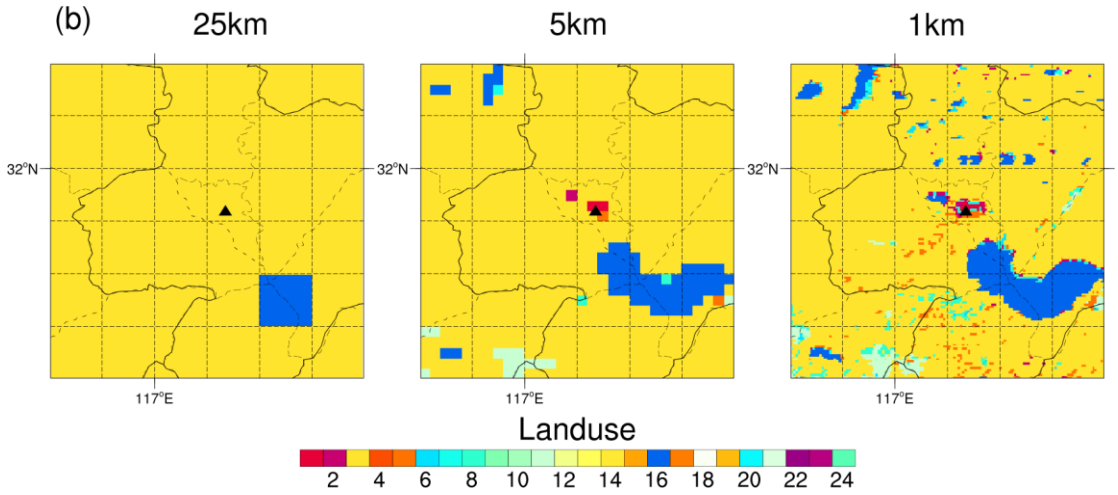

Figure S2. The spatial distribution of the default USGS land use category data in WRF in the study area for 25-km (left), 5-km (middle), and 1-km (right) resolution simulations, respectively. The solid black triangle indicates the location of the USTC site.

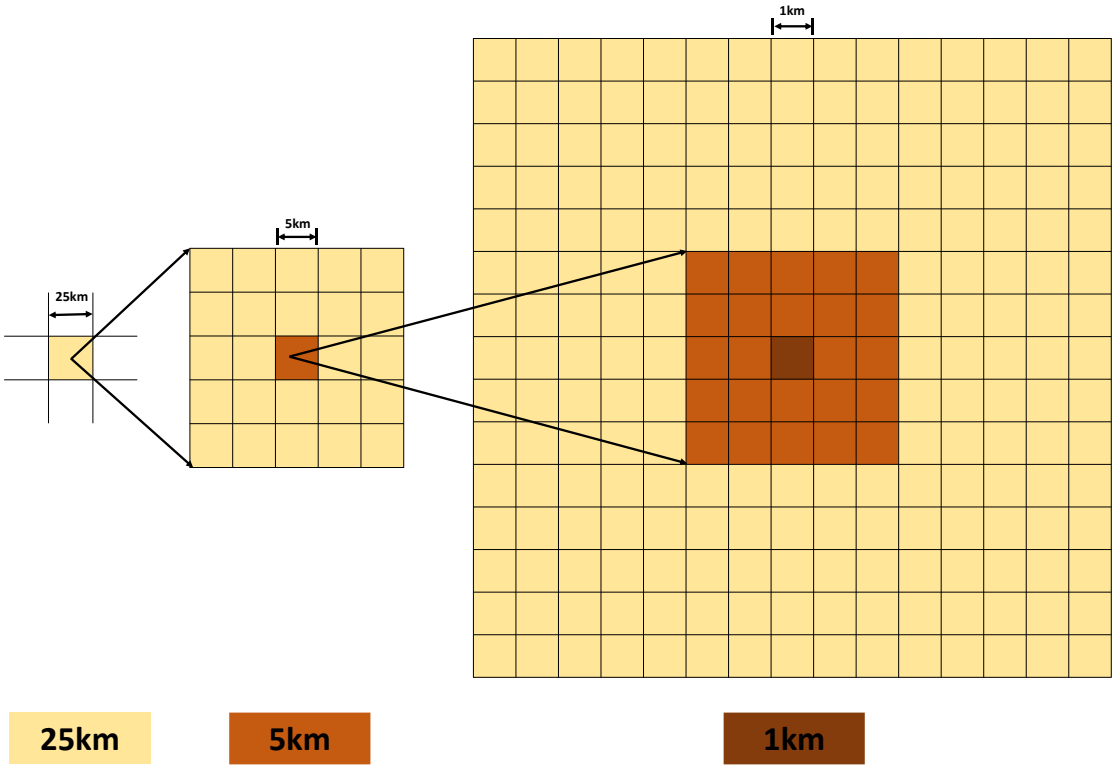

Figure S3. Conceptual subdivision of a coarse grid cell from the 25-km grid into smaller grid points for the finer grids. Each 25-km grid cell is subdivided into 25 5-km grid cells. Each of the 5-km grid cells are further refined into 25 1-km grid cells for a total of 625 1-km grid cells per 25-km cell. The solid black triangle indicates the location of the USTC site.

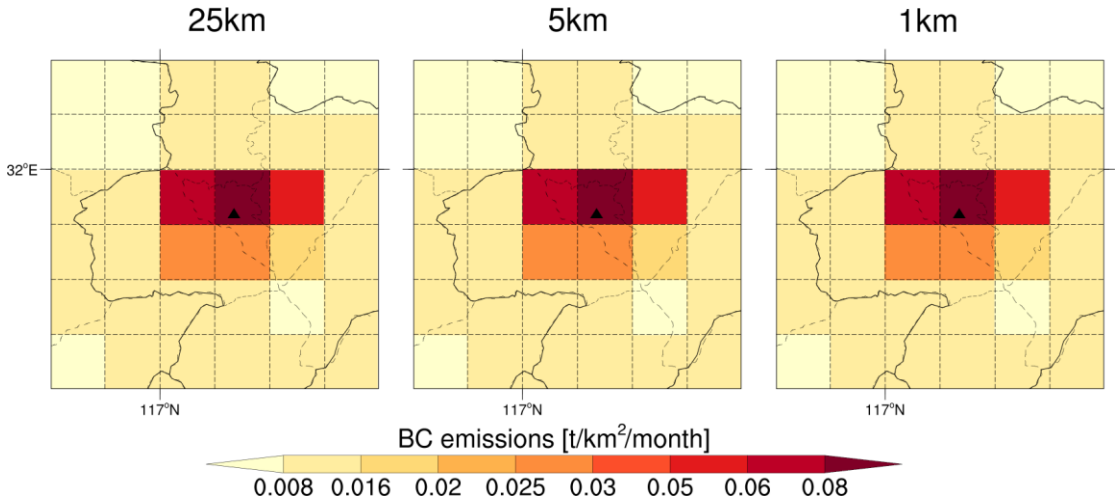

Figure S4. Spatial distribution of BC emissions in the study area for 25-km (left), 5-km (middle), and 1-km (right) resolution simulations, respectively. The solid black triangle indicates the location of the USTC site.

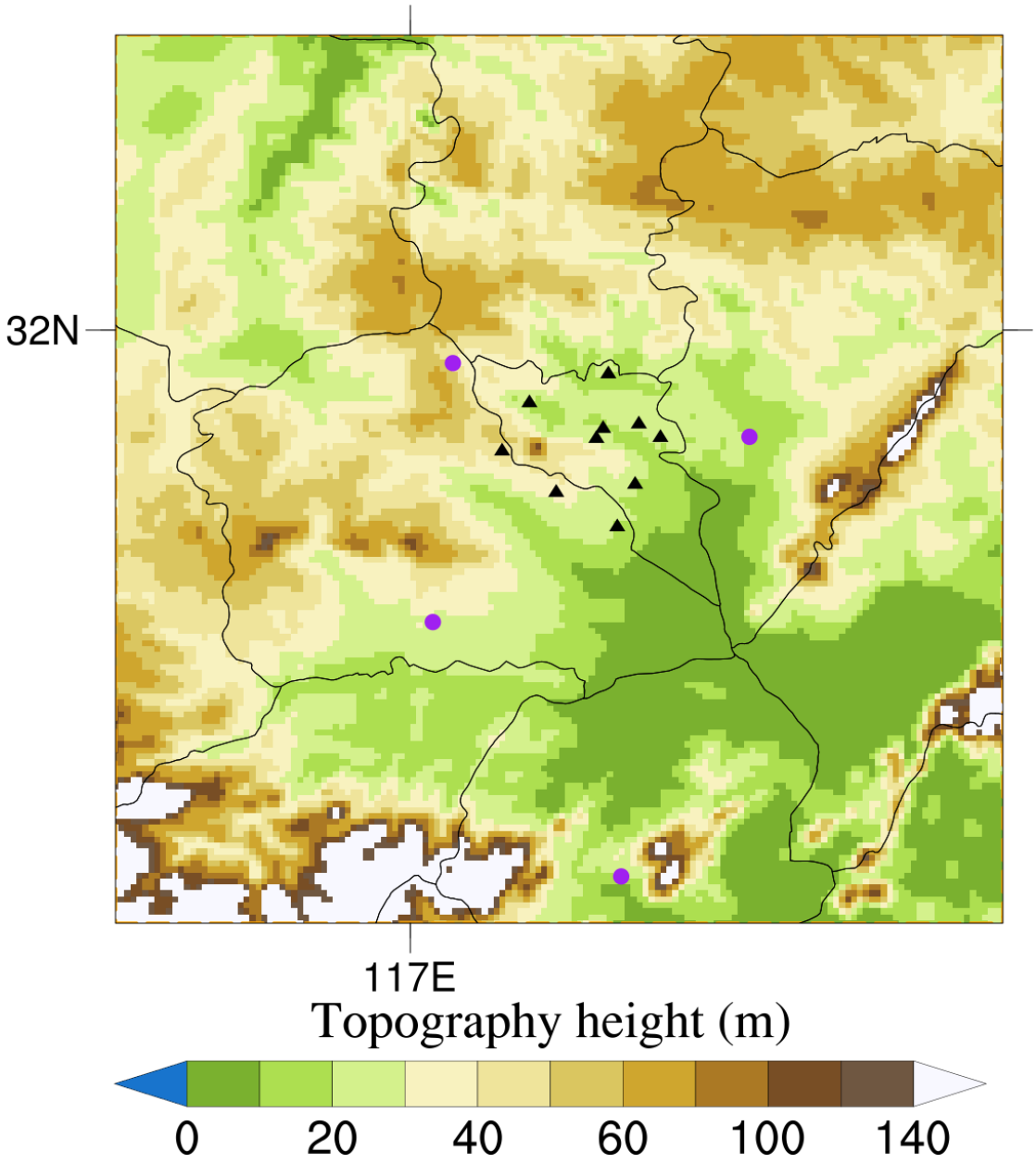

Figure S5. Spatial distributions of 4 MEP and 10 AWS sites used in this study. Solid black triangles indicate MEP monitoring sites, and purple solid dots indicate AWSs locations.

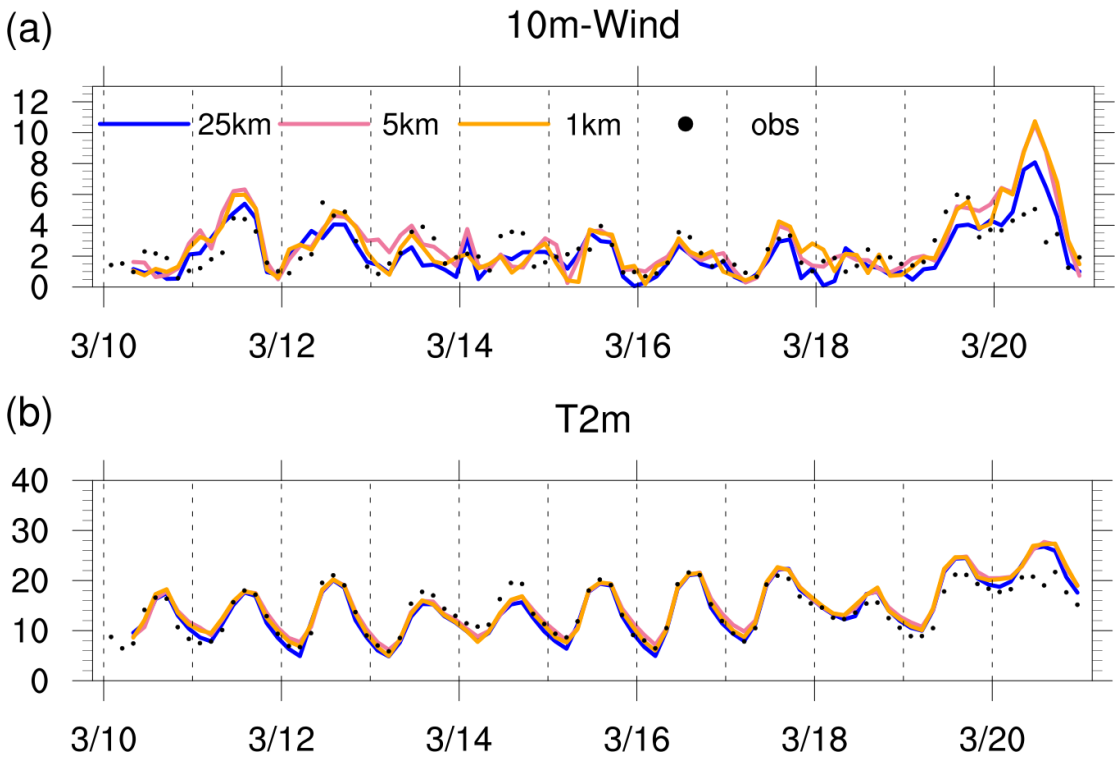

Figure S6. Time series averaged over 4 AWS sites in Hefei of observed (black dot) and simulated wind speed at 8 m (top, unit: m s-1) and temperature at 2 m (middle, unit: ℃) for 25-km (solid blue line) resolution, 5-km (solid pink line) resolution, and 1-km (solid orange line), respectively.

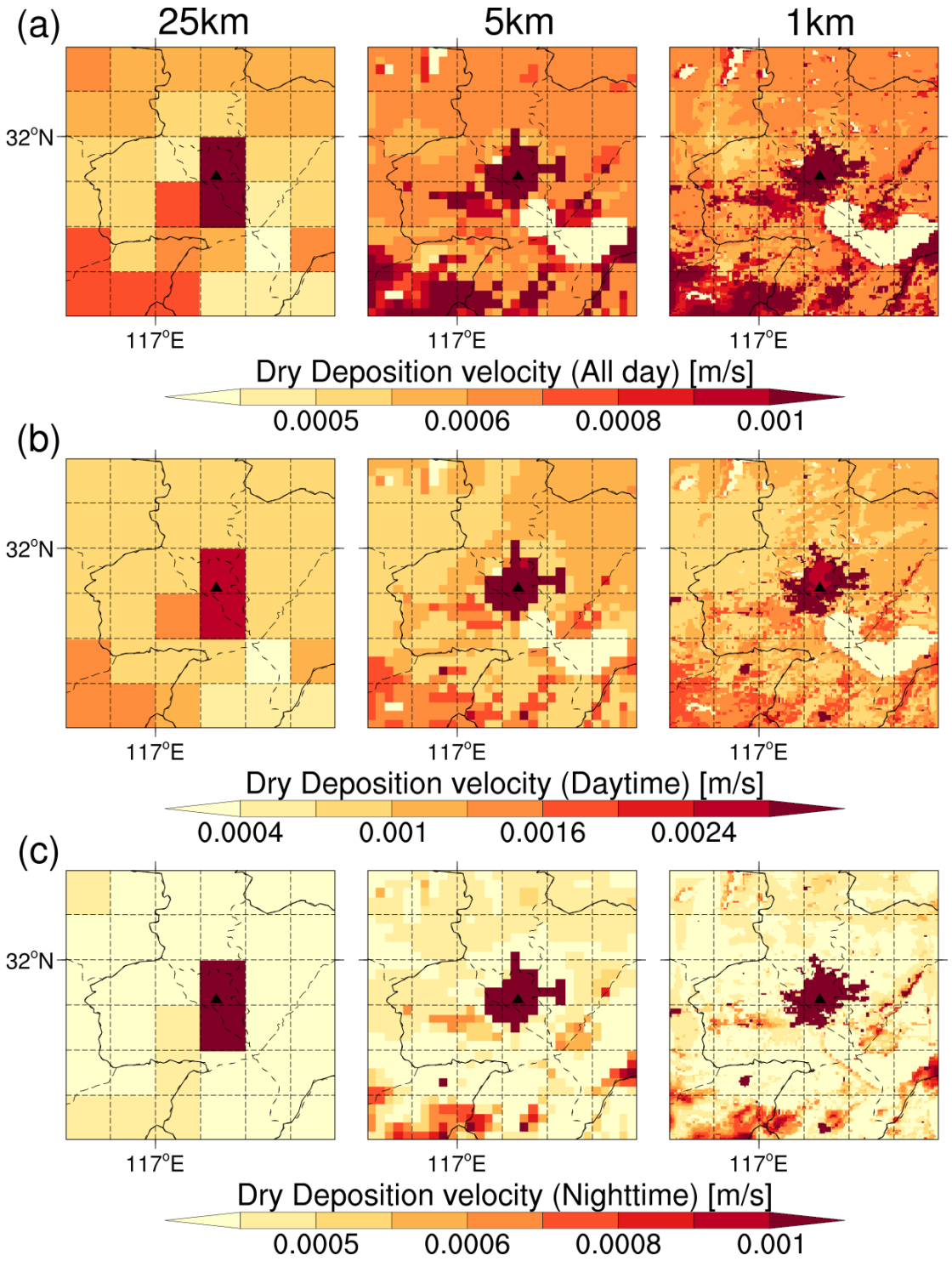

Figure S7. Spatial distribution of the dry deposition velocity in the study area for 25-km (left), 5-km (middle), and 1-km (right) resolution simulations of the whole day (top), the daytime (middle), and the nighttime (bottom), respectively. The solid black triangle indicates the location of the USTC site.

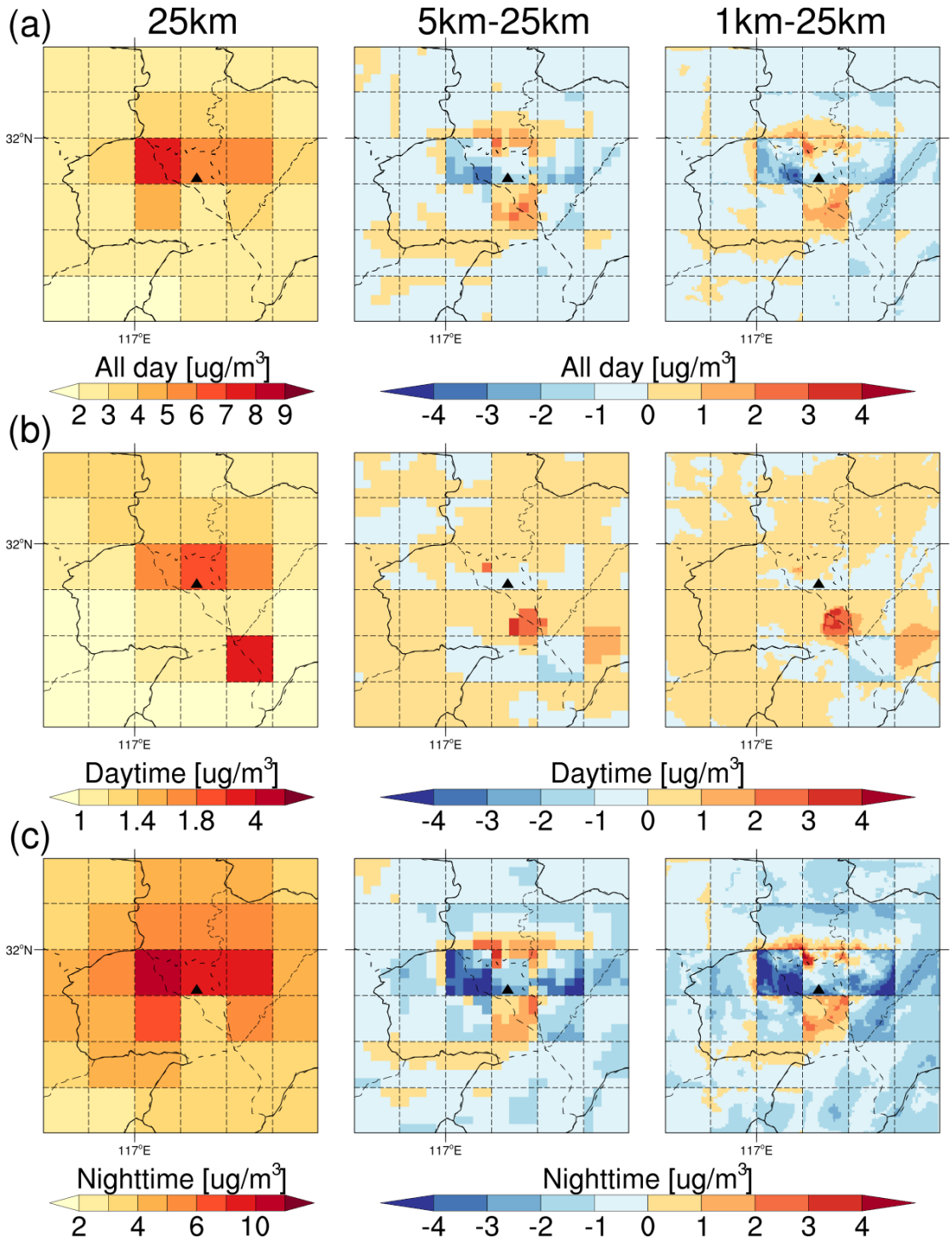

Figure S8. Spatial distribution of the BC surface concentration in the study area for 25-km resolution (left), the difference between 25-km and 5-km resolutions (middle), and the difference between 25-km and 1-km (right) resolutions of the whole day (top), the daytime (middle), and the nighttime (bottom), respectively. The solid black triangle indicates the location of the USTC site.

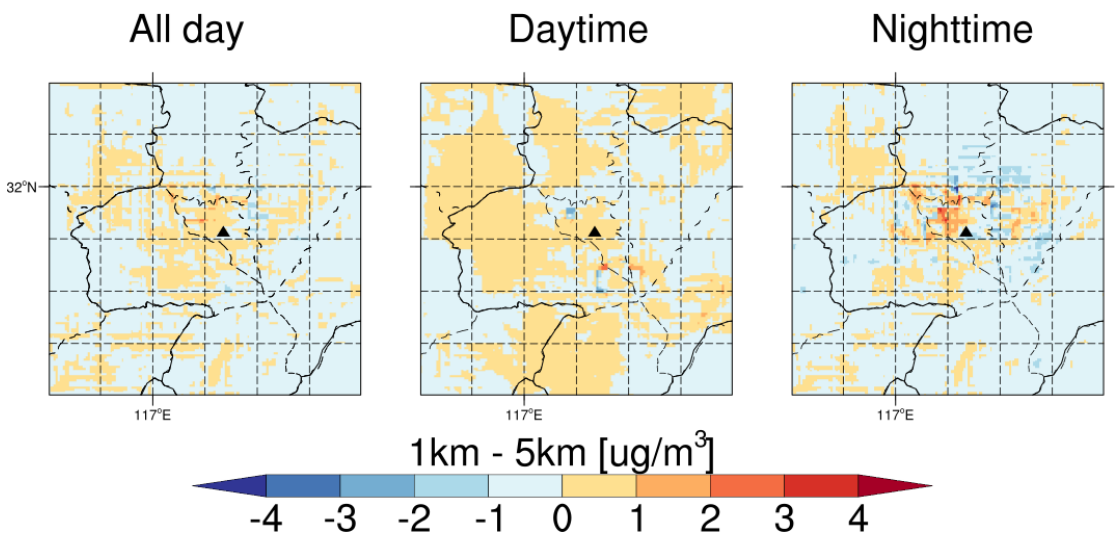

Figure S9. Spatial distribution of the differences in BC surface concentrations between 1-km and 5-km resolutions in the study area of the whole day (left), the daytime (middle), and the nighttime (right), respectively. The solid black triangle indicates the location of the USTC site.

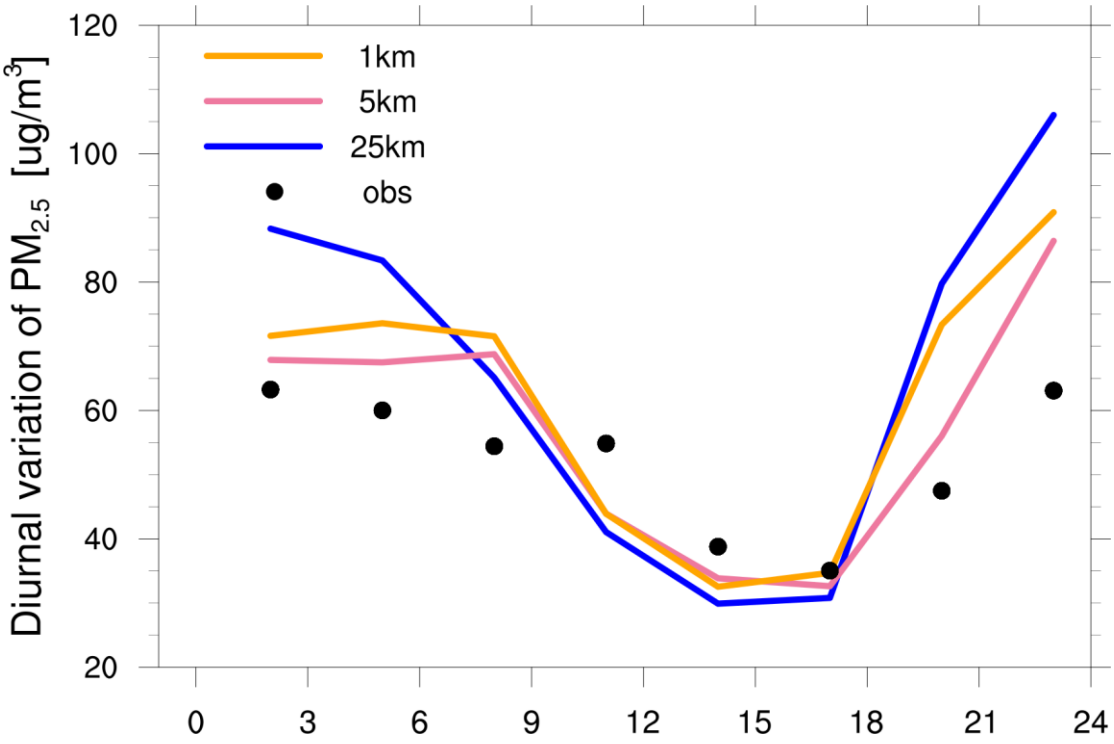

Figure S10. Diurnal variation of $PM_{2.5}$ surface concentrations within 24 h averaged over 10 MEP sites in Hefei during the study period for 25-km (solid blue line), 5-km (solid pink line), and 1-km (solid orange line) resolution simulations and observations (black dot). Both the simulated results and observations are sampled at the model output frequency, i.e., 3-hourly.

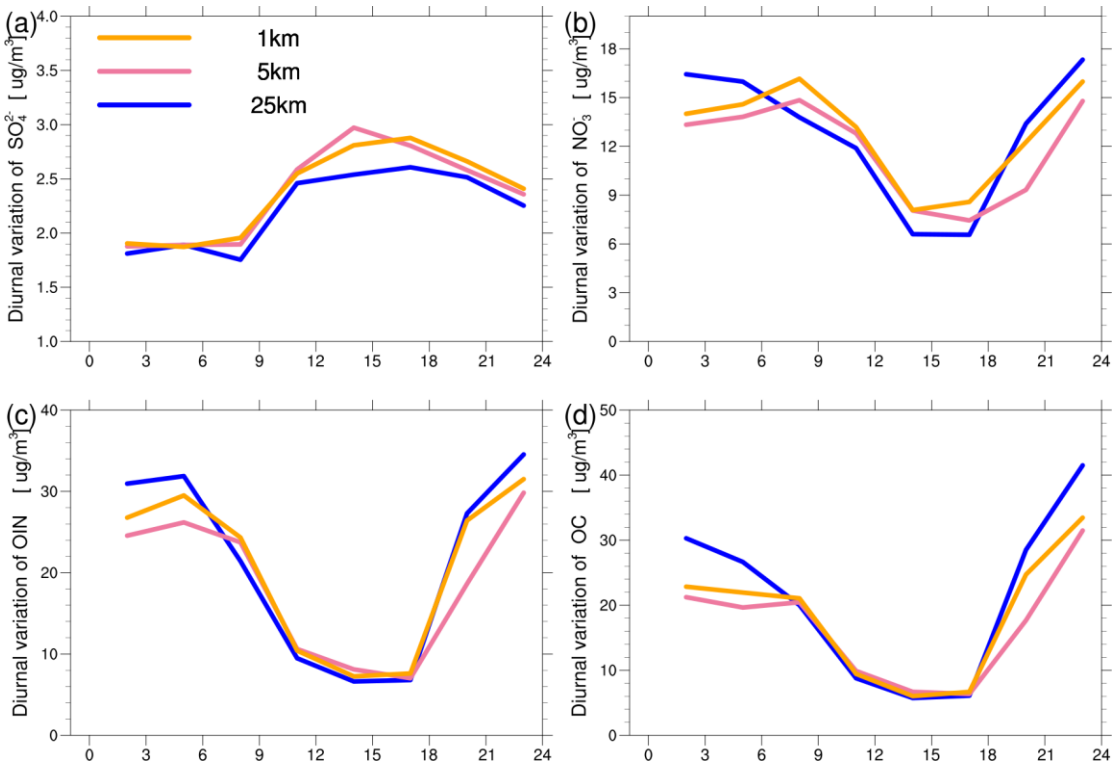

Figure S11. Diurnal variation of (a) $\mathbf{SO_4^{2-}}$, (b) $\mathbf{NO_3^-}$, (c) OIN, and (d) OC surface concentrations within 24 h averaged over 10 MEP sites in Hefei during the study period for 25-km (solid blue line), 5-km (solid pink line), and 1-km (solid orange line) resolution simulations. The simulated results are sampled at the model output frequency, i.e., 3-hourly.

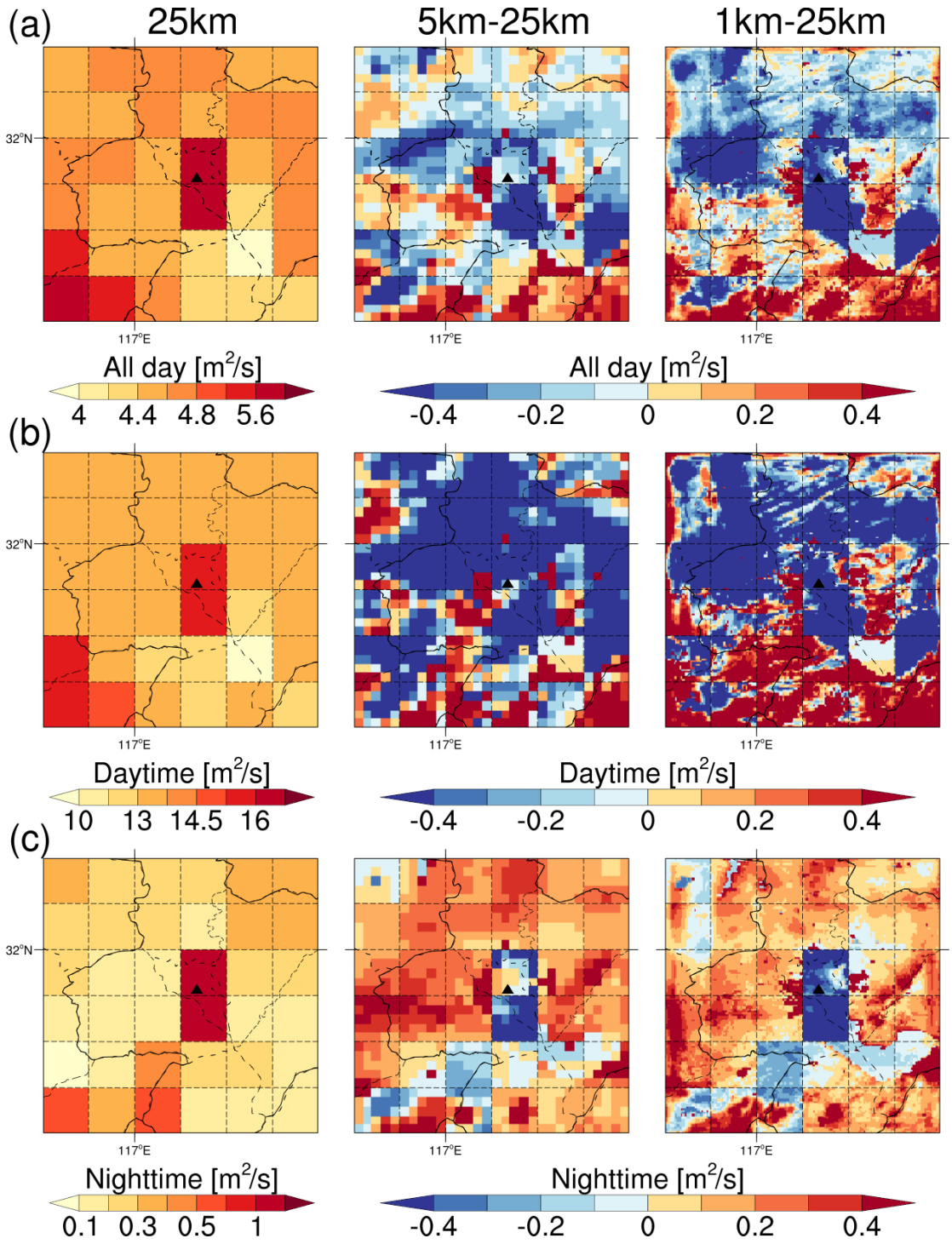

Figure S12. Spatial distribution of PBL mixing coefficients in the study area for 25-km resolution (left), the difference between 25-km and 5-km resolutions (middle), and the difference between 25-km and 1-km (right) resolutions of the whole day (top), the daytime (middle), and the nighttime (bottom), respectively. The solid black triangle indicates the location of the USTC site.

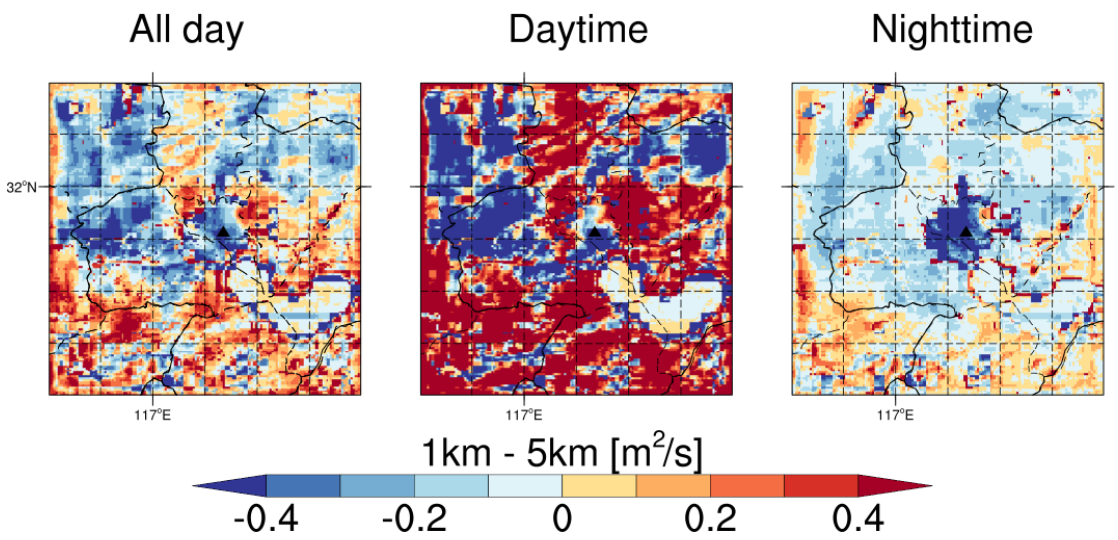

Figure S13. Spatial distribution of the differences in PBL mixing coefficients between 1-km and 5-km resolutions in the study area of the whole day (left), the daytime (middle), and the nighttime (right), respectively. The solid black triangle indicates the location of the USTC site.

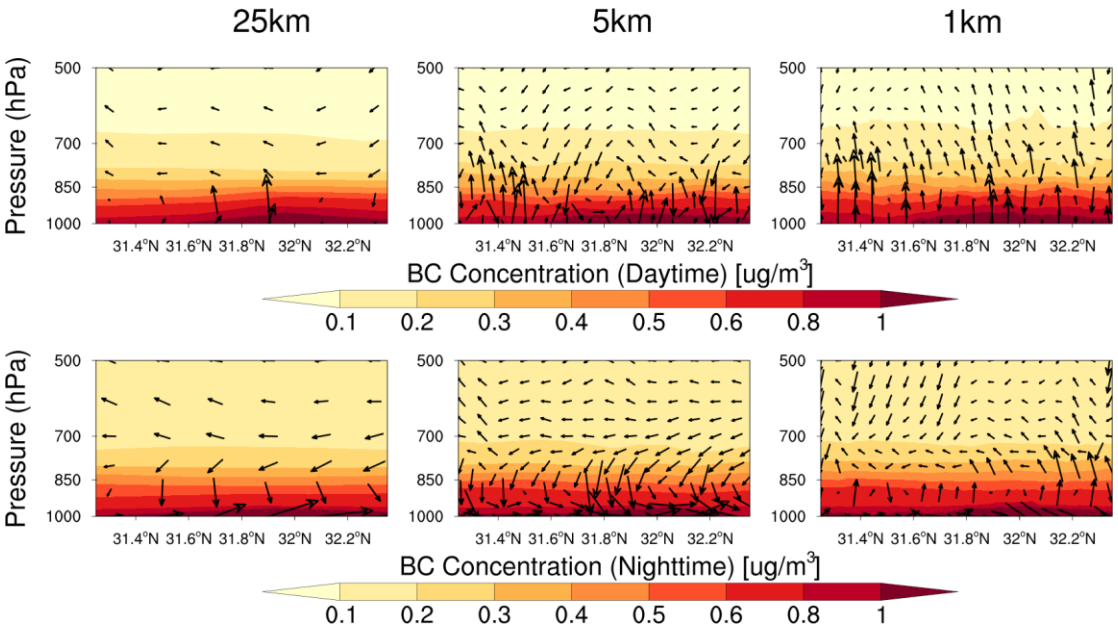

Figure S14. The latitude-pressure cross section of BC concentrations and wind speed flux along the USTC site for 25-km (left), 5-km (middle), and 1-km (right) resolution simulations of the daytime (top), and the nighttime (bottom), respectively. Vector arrows are the combination of wind speed fluxes v and w, with the vertical wind speed flux being multiplied by 100 for visibility. The shaded contours represent BC concentrations at each pressure level.

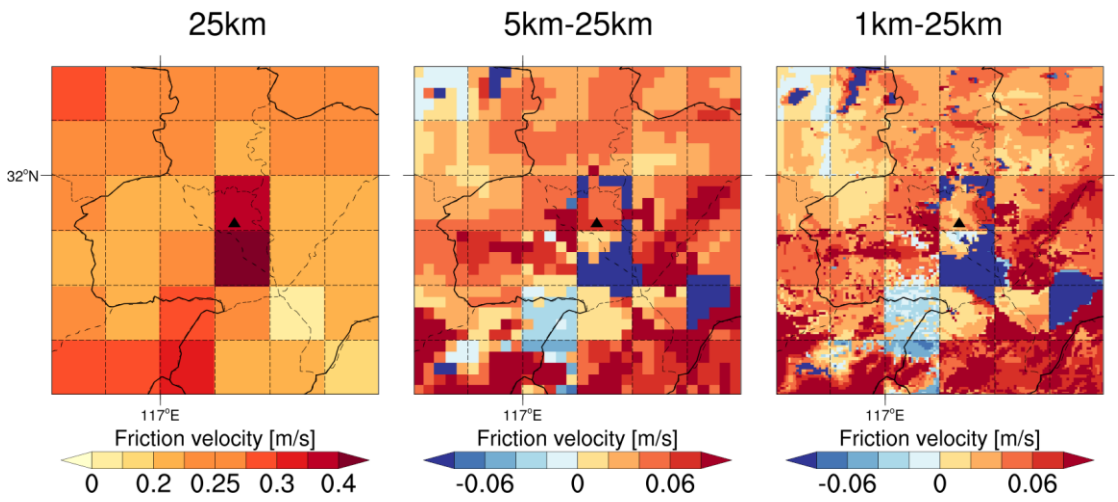

Figure S15. Spatial distribution of the friction velocity in the study area for 25-km resolution (left), the difference between 25-km and 5-km resolutions (middle), and the difference between 25-km and 1-km resolutions (right) simulations of the whole day, respectively. The solid black triangle indicates the location of the USTC site.

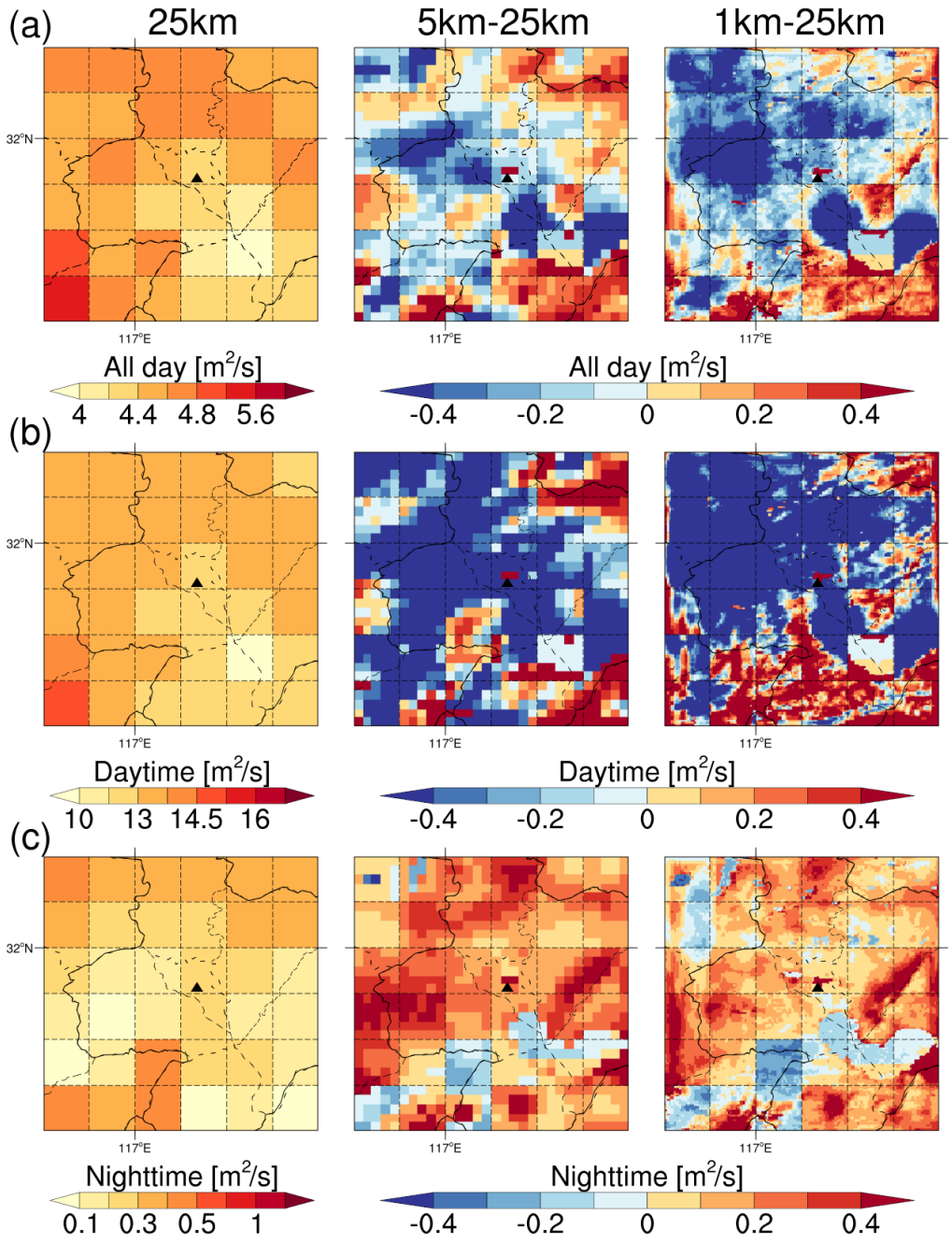

Figure S16. Spatial distribution of PBL mixing coefficients in the study area for 25-km resolution (left), the difference between 25-km and 5-km resolutions (middle), and the difference between 25-km and 1-km (right) resolutions of the whole day (top), the daytime (middle), and the nighttime (bottom), respectively. The solid black triangle indicates the location of the USTC site. The simulation results are from the sensitivity experiments.

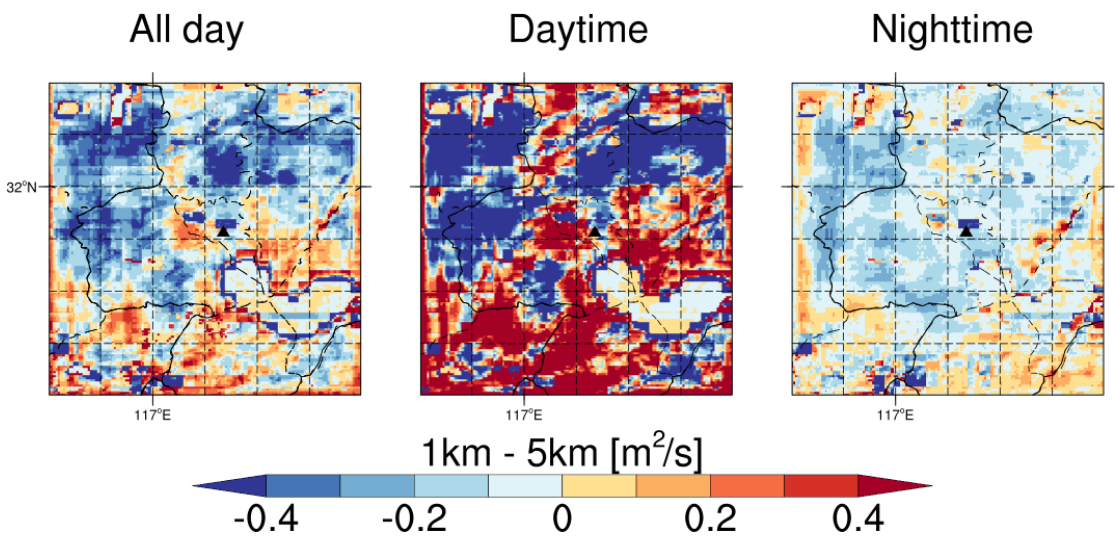

Figure S17. Spatial distribution of the differences in PBL mixing coefficients between 1-km and 5-km resolutions in the study area of the whole day (left), the daytime (middle), and the nighttime (right), respectively. The solid black triangle indicates the location of the USTC site. The simulation results are from the sensitivity experiments.

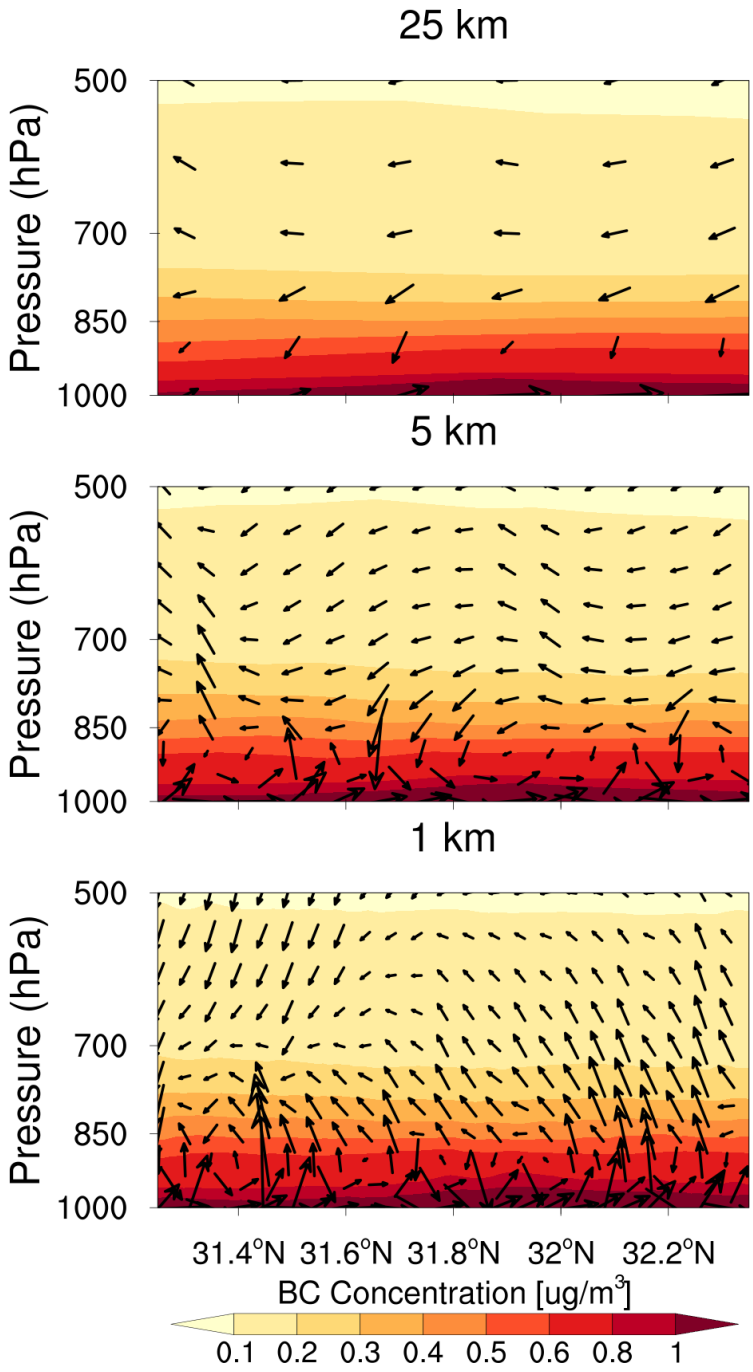

Figure S18. The latitude-pressure cross section of BC concentrations and wind speed flux along the USTC site for 25-km (top), 5-km (middle), and 1-km (bottom) resolution simulations of the whole day, respectively. Vector arrows are the combination of wind speed fluxes v and w, with the vertical wind speed flux being multiplied by 100 for visibility. The shaded contours represent BC concentrations at each pressure level. The simulation results are from the sensitivity experiments.

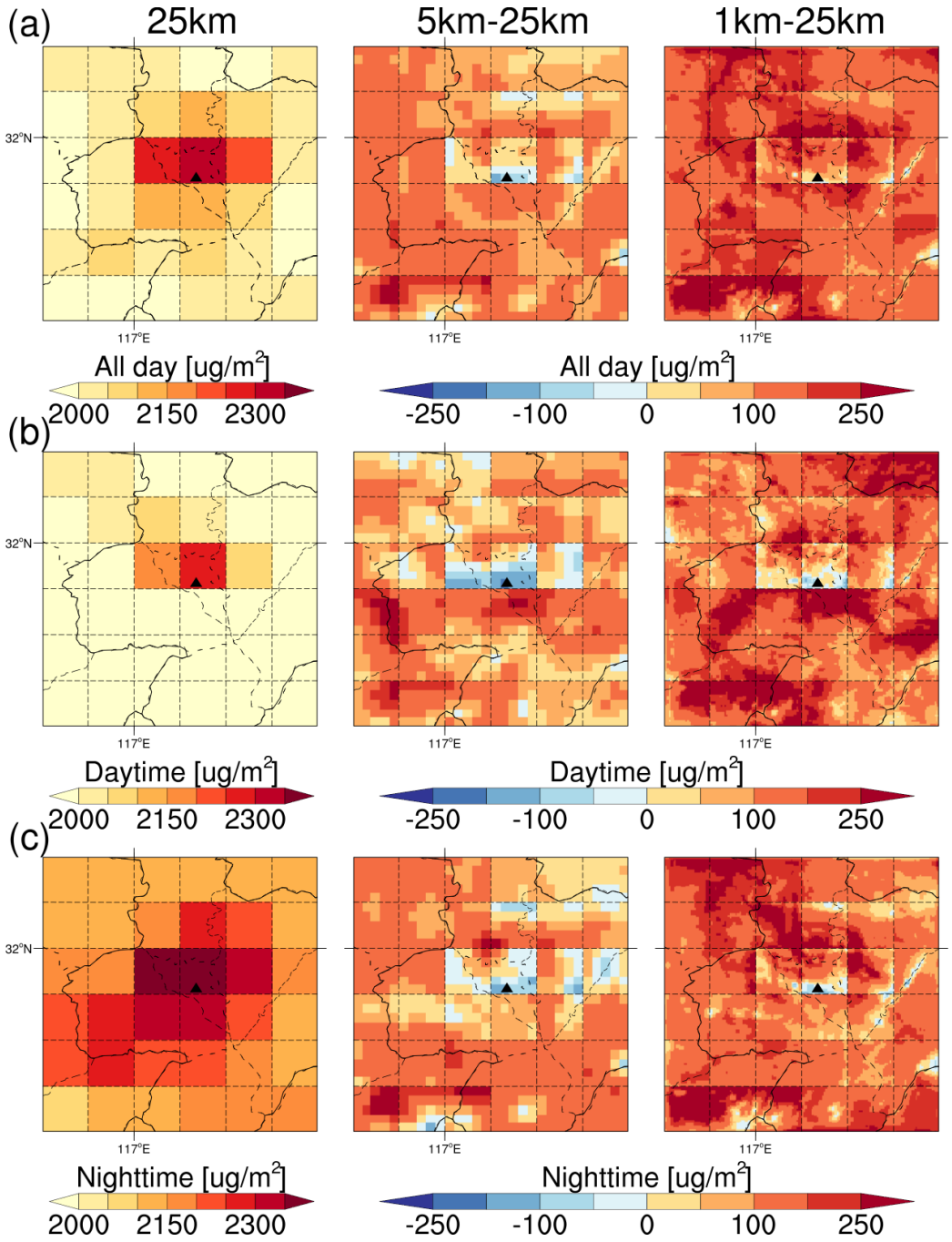

Figure S19. Spatial distribution of the BC column concentration in the study area for 25-km resolution (left), the difference between 25-km and 5-km resolutions (middle), and the difference between 25-km and 1-km (right) resolutions of the whole day (top), the daytime (middle), and the nighttime (bottom), respectively. The solid black triangle indicates the location of the USTC site.

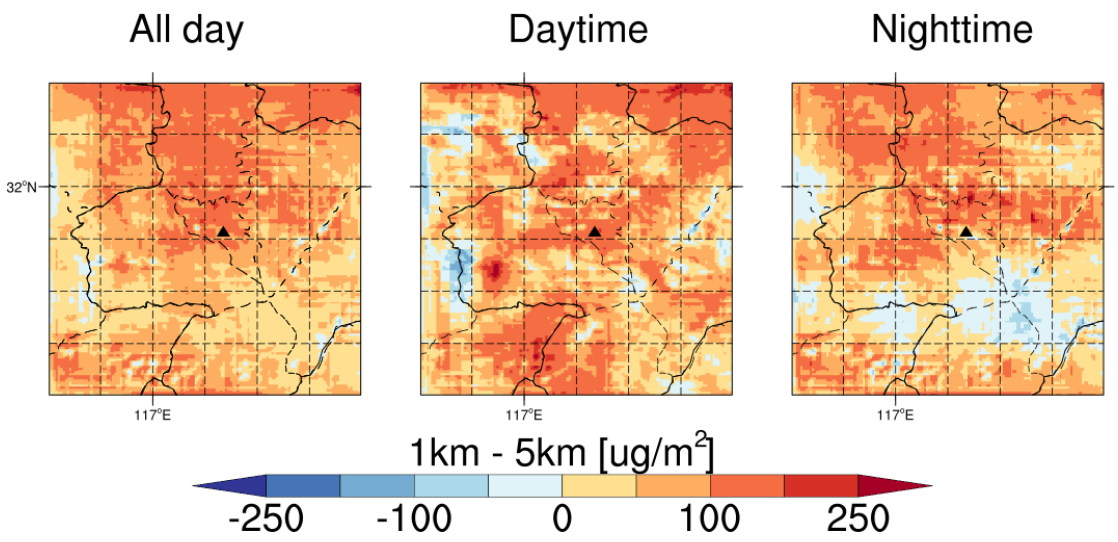

Figure S20. Spatial distribution of the differences in BC column concentrations between 1-km and 5-km resolutions in the study area of the whole day (left), the daytime (middle), and the nighttime (right), respectively. The solid black triangle indicates the location of the USTC site.